# High-Fidelity Voltage-Behind-Reactance Model of Electrically Excited Synchronous Machines Using Flux Maps

IEEE Open Journal of
Industry Applications

Received 3 April 2025; revised 27 June 2025; accepted 4 August 2025. Date of publication 11 August 2025;
date of current version 27 August 2025.

*Digital Object Identifier 10.1109/OJIA.2025.3597812*

# High-Fidelity Voltage-Behind-Reactance Model of Electrically Excited Synchronous Machines Using Flux Maps

**ALESSANDRO IONTA (Graduate Student Member, IEEE), SANDRO RUBINO (Member, IEEE), FEDERICA GRAFFEO (Member, IEEE), AND RADU BOJOI (Fellow, IEEE)**

Dipartimento Energia "G. Ferraris", Politecnico di Torino, 10129 Torino, Italy

CORRESPONDING AUTHOR: ALESSANDRO IONTA (email: alessandro.ionta@polito.it).

**ABSTRACT** Electrically excited synchronous machines (EESMs) have historically been used as efficient and reliable synchronous generators. However, the actual need for cost-effective, sustainable motors without rare-earth magnets has notably increased the interest in EESMs, which are considered a valid replacement for permanent magnet synchronous machines (PMSMs) in electrified powertrains. As the electrical machines employed in automotive applications exhibit deep magnetic saturation, the EESM introduces significant challenges in properly modeling the magnetic behavior, especially considering the cross-coupling effects between stator and rotor. EESM-based electrical drive development requires accurate circuital models to predict EESM behavior. Therefore, this article proposes a novel voltage-behind-reactance (VBR) model based on flux maps provided by finite element analysis (FEA) or experimental identification procedures. The proposed VBR model has been validated in simulation and experimentally on a commercial 100 kW EESM currently used on the Renault Zoe EV R135, demonstrating its potential for accurately modeling EESMs designed for traction applications.

**INDEX TERMS** Armature reaction, circuital modeling, cross-coupling, electrically excited synchronous machine (EESM), flux maps, voltage-behind-reactance (VBR).

## I. INTRODUCTION

Today, the permanent magnet synchronous machine (PMSM) is the dominant solution used in automotive applications due to its superior power density and efficiency [1]. The nonlinear magnetic behavior of PMSMs has been rigorously studied using the current-to-flux and flux-to-current maps [2], [3], [4], [5], denominated in this article as *direct* and *inverse* flux maps, respectively.

Recently, the growing interest in rare-earth-free electrical machines as an alternative technology for traction applications has driven the adaptation of methods that employ direct and inverse flux maps to study the magnetic behavior of electrical machines to electrically excited synchronous machines (EESMs) [6], [7], [8], [9]. This class of machines, also referred to as wound-field synchronous machines (WFSM), incorporates a rotor winding to generate the excitation field, eliminating the need for permanent magnets and also mitigating the risks associated with demagnetization and uncontrolled generation. Furthermore, the EESM provides an additional degree of control, as the flux can be regulated through the rotor field current. This capability facilitates constant power operation over a broad speed range and enables effective flux weakening while maintaining high efficiency.

The simulation of electrical powertrains requires a detailed analysis of the power converter and the machine. Circuit-based models are a viable solution for this purpose. For such models, it is beneficial to reformulate the machine's equations in the so-called voltage-behind-reactance (VBR) form [10]. The VBR formulation decouples the synchronous machine model into stator and rotor subsystems. The stator subsystem is expressed in the $dq$ rotor reference frame, using flux linkages as independent variables. The rotor dynamic equations are explicitly stated in state model form, while the stator

equations are presented in circuit form. A significant advantage of VBR models is their straightforward integration into circuit-based simulation software, such as piece-wise linear electrical circuit simulation (PLECS) [11], since the machine windings are represented by branches that can be connected in the appropriate topology [12].

Over the past decades, EESMs have primarily been used as generators supplying dc loads through rectifiers in various applications. Consequently, the design and modeling approaches of these machines have been tailored to this specific use case, as evidenced in [13], [14], [15], [16]. In these models, nonlinearities are approximated using a magnetic saturation curve, which defines the relationship between the magnetizing current and the corresponding magnetizing flux linkage [17], [18], [19]. However, a novel VBR circuital model is required to account for the characteristics of EESMs employed as traction motors, mainly motivated by their extensive usage in deep saturation [20], [21], [22]. For enhanced accuracy in dynamic modeling, the relationships between flux linkages and machine currents can be represented using mapping techniques. These mappings establish a direct correlation between stator and rotor currents and the associated fluxes, thereby eliminating the need for approximating functions to model nonlinearities. A comprehensive analysis of the magnetic behavior under cross and deep saturation needs detailed flux maps of the motor, including rotor flux. This assumption is particularly realistic in the automotive traction field, where finite element analysis (FEA) software is extensively used to identify flux maps [23]. These maps can be implemented numerically using either fitting functions or look-up tables (LUTs), both approaches achieving similar or equivalent accuracy [24].

Moreover, VBR models of EESMs require accurate estimation of the stator parameters like resistance and leakage inductance. In particular, a reliable estimation of the stator leakage inductance and its saturation is not straightforward to obtain through analytical calculations [25], [26]. However, the accurate estimation of this parameter for EESMs still represents an open issue in the literature.

According to the aforementioned scenario and to respond to the need for new models for saturated EESMs for traction, the primary goal of this article is to propose a new accurate VBR model for EESM, based on the direct flux maps. The proposed VBR model brings added value to the existing literature as follows.

1) It correctly accounts for the magnetic coupling between the stator and the rotor to depict the armature reaction, i.e., the effect of the stator currents inducing voltage on the rotor circuit. An accurate modeling of the armature reaction is guaranteed under significant magnetic saturation thanks to the implementation of complete flux maps replicating the exact current-to-flux relationships of stator and rotor windings.
2) It represents both stator and rotor with VBR circuital formulation able to simulate rotor open circuit scenarios.

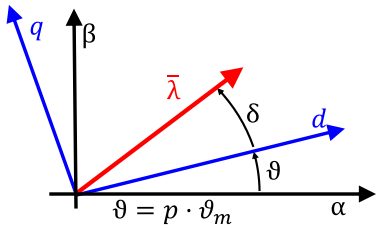


**FIGURE 1. Schematic view of the system coordinates for a generic ac motor.**

3) It considers properly, through mathematical manipulation of the flux maps, the stator leakage inductance.

The validation of the proposed model has been performed by comparing experimental results obtained with a 100 kW EESM from the Renault Zoe EV R135 with the simulation results carried out with the PLECS simulator. In addition, a comparison with [15] is included, highlighting the limitations of this modeling approach in adequately representing the magnetic behavior of modern EESMs designed for traction applications.

The rest of this article is organized as follows. Section II presents the machine modeling. A comprehensive literature review on EESM models is provided in Section III, while in Sections IV and V, the new VBR formulation and the elaboration of the stator leakage flux are retrieved, respectively. Section VI and Section VII contains the simulation and experimental validation. Finally, Section VIII concludes this article.

## II. EESM MODELING

Voltage and flux linkage equations of synchronous machines can be written in both stator and rotor coordinates that are defined in Fig. 1. According to the literature [27], the voltage ($dq$) model of a synchronous machine can be computed as

$$\begin{cases} v_d = R_s \cdot i_d + \frac{d}{dt}\lambda_d - \omega \cdot \lambda_q \\ v_d = R_s \cdot i_q + \frac{d}{dt}\lambda_q + \omega \cdot \lambda_d \end{cases}. \tag{1}$$

The subscripts of the stator vectors for voltage $v$, current $i$, and flux linkage $\lambda$ indicate their respective $dq$ components, with $R_s$ representing the stator resistance and $\omega$ the electrical speed.

The stator current equations of a EESM are quite challenging to express analytically, due to the magnetic saturation phenomena involving both stator and rotor. For large current values, iron saturation causes the magnetic flux to deviate from a linear relationship with respect to current. As a result, the mapping between each current and its corresponding flux component becomes highly nonlinear. Furthermore, since both flux components share the same magnetic path, they exert mutual influence on one another. Consequently, saturation in one flux component can lead to a reduction in the other, a phenomenon known as cross-coupling [28]. To accurately capture this effect in EESMs, each flux component must be

modeled as a function of stator current $dq$ components and rotor current. However, if assuming machine $dq$ inductances dependent on the the stator $dq$ currents and also on the rotor field current ($i_f$), the current-to-flux relationships of a EESM are expressed in rotor $dq$ coordinates as follows:

$$\begin{cases} \lambda_d = L_{dd}(i_d, i_q, i_f) \cdot i_d + L_{dq}(i_d, i_q, i_f) \cdot i_q \\ \qquad + L_{df}(i_d, i_q, i_f) \cdot i_f \\ \lambda_q = L_{qd}(i_d, i_q, i_f) \cdot i_d + L_{qq}(i_d, i_q, i_f) \cdot i_q \\ \qquad + L_{qf}(i_d, i_q, i_f) \cdot i_f \end{cases} \tag{2}$$

where $L_{dd}$ and $L_{qq}$ are the machine's self-inductances along the corresponding $dq$ axes, while $L_{dq}$ and $L_{qd}$ are the cross-inductances between the stator $dq$ axes and $L_{df}$ and $L_{qf}$ are the cross-inductances between the stator $dq$ axes and the rotor field circuit.

The unified equation of the electromagnetic torque $T$ is

$$T = \frac{3}{2} \cdot p \cdot (\bar{\lambda} \times \bar{i}) = \frac{3}{2} \cdot p \cdot (\lambda_d \cdot i_q - \lambda_q \cdot i_d) \tag{3}$$

where $p$ is the pole pair number. As can be seen from (1) to (3), the EESM model is totally similar of any other generic ac motor, the difference lies in the added dependencies of the flux linkage (2) to the rotor field current $i_f$.

### A. ROTOR MODEL

The rotor voltage equation is expressed as

$$v_f = R_f \cdot i_f + \frac{d}{dt}\lambda_f \tag{4}$$

where $R_f$ is the rotor resistance and $\lambda_f$ is the flux linkage at the rotor side.

As happens for (2), the cross-inductances between stator and rotor have to be taken into account as follows:

$$\lambda_f = L_{fd}(i_d, i_q, i_f) \cdot i_d + L_{fq}(i_d, i_q, i_f) \cdot i_q + L_{ff}(i_d, i_q, i_f) \cdot i_f \tag{5}$$

where $L_{ff}$ is the machine rotor self-inductance while $L_{fd}$ and $L_{fq}$ are the machine's cross-inductances between the rotor and the stator $dq$ axes.

## III. LITERATURE ANALYSIS

Various methods are currently reported in the state-of-the-art modeling of synchronous machine for power system studies [29], [30], [31], [32]. In the following, a brief analysis of the available models for EESM is provided, highlighting their advantages and disadvantages with respect to the proposed model (see Table 1).

A first attempt in EESM modeling can be done by expressing the stator magnetic model as for PMSM [33], [34], [35], and replacing the magnets flux linkage with a field flux linkage that depends on the rotor field current $i_f$ [36]. The $dq$-model is expressed following the relationship (1). Accordingly to (2), the flux model is more precisely represented as a 3-D mapping as follows:

$$f_\lambda : (i_d, i_q, i_f) \rightarrow (\lambda_d, \lambda_q). \tag{6}$$

**TABLE 1. EESM Model Formulations**

| | Stator interface | Rotor interface | Cross-coupling (stator-rotor) |
|---|---|---|---|
| Flux maps inversion [6], [9] | Indirect | Indirect | Accurate |
| Stator-VBR [14], [10], [12], [13] [19], [32], [37] | Direct | Indirect | Inaccurate |
| Full-VBR [15], [31], [38] | Direct | Direct | Inaccurate |
| Proposed VBR | Direct | Direct | Accurate |

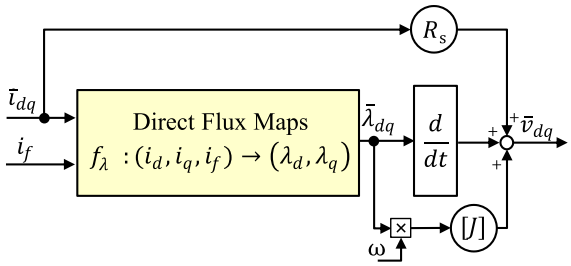


**FIGURE 2. *dq* model with imposed rotor current for EESM.**

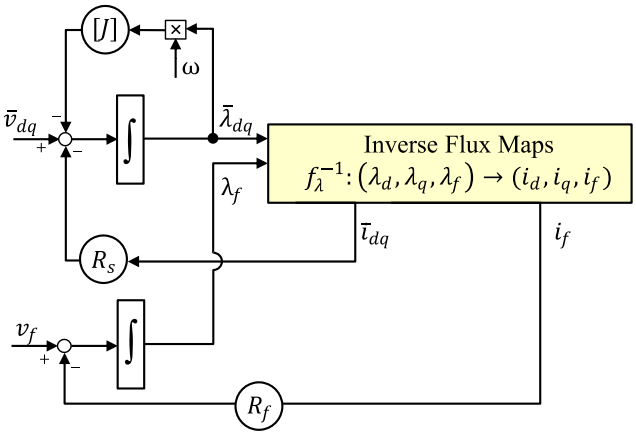


**FIGURE 3. Inverse flux maps-based model for EESM.**

Consequently, $i_f$ can be only imposed a priori, completely neglecting the rotor magnetic behavior (see Fig. 2).

The nonlinear magnetic behavior of PMSMs has been thoroughly investigated using inverse flux maps expressed as follows:

$$f_\lambda^{-1} : (\lambda_d, \lambda_q) \rightarrow (i_d, i_q). \tag{7}$$

This approach can be also applied to EESMs [9], but with increased complexity due to the additional variable given by the rotor field current, resulting in a 3-D system described by the following:

$$f_\lambda^{-1} : (\lambda_d, \lambda_q, \lambda_f) \rightarrow (i_d, i_q, i_f). \tag{8}$$

A procedure for the inversion of $n$-dimensional maps is described in [6] and [9]. If the rotor flux maps are included, the complete machine behavior comprehensive of the rotor can be derived, as shown in Fig. 3. The main drawback of this type

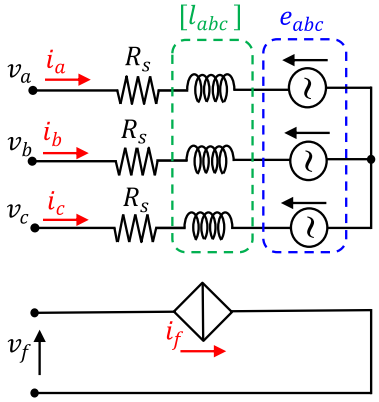


**FIGURE 4.** Stator-VBR model for EESM.

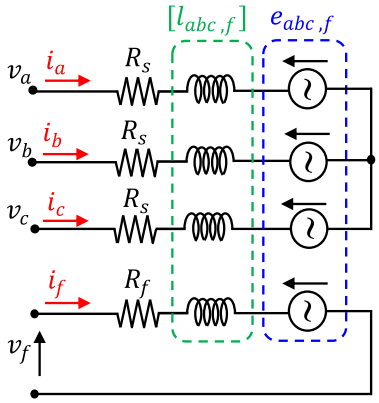


**FIGURE 5.** Full-VBR model for EESM.

of modeling is its inability to be adapted into a circuit-based form.

Another approach consists of the application of the VBR formulation. This model demonstrates computational efficiency, flexibility regarding stator winding configurations, and compatibility with both circuit-based and differential equation-based simulation methodologies.

The description of the application of the classical VBR formulation to EESM is presented in [14]. This type of representation is also called Stator-VBR for its characteristic on having only the stator represented in a circuital form. The Stator-VBR allows direct network-machine interfacing at the stator terminals. In this model, to interface the rotor to an arbitrary network, a controlled current source is used (see Fig. 4). Therefore, this methodology implies the existence of some constraints on possible simulation scenarios; for example, an open-circuit on the rotor side cannot be properly simulated.

The approach presented in [15] intends representing both stator and rotor with VBR circuital formulation, for this reason it is called Full-VBR. As described in [15], the interfacing circuit model is represented by a 4-by-4 inductance matrix, with rotor position-dependent off-diagonal terms coupling the field and the stator (see Fig. 5).

Although many other works in the literature discuss different Stator- and Full-VBR formulations, comprising constant or variable parameter approaches [10], [12], [13], [19], [31], [32], [37], [38], none of these can accurately replicate the cross-coupling effects between the stator and rotor in significant magnetic saturation conditions. Indeed, nonlinearities are approximated using a magnetic saturation curve [16], [39]. Therefore, the formulations proposed in the literature are not able to provide the precise magnetic relationship described in (2) and (5). This simplification makes the model insufficiently accurate for representing the cross-coupling effects between the stator and rotor in significant magnetic saturation conditions.

The modern interest in EESMs as an alternative to PMSMs for traction applications has emphasized the need for more precise stator-rotor coupling modeling.

## IV. PROPOSED VBR MODEL

Following the advantages of the formulations existing in the literature, the developed VBR model is defined with an interfacing circuit consisting of a 4-by-4 incremental inductance matrix, which includes stator and rotor terms. The inductances are dependent on $(i_d, i_q, i_f)$ and consequently on the rotor position, including terms coupling the rotor and the stator. Therefore, the interfacing circuit parameters are variable. The novel inductances calculation approach through the flux maps, detailed in the following, allows this definition.

### A. STATOR-VBR FORMULATION WITH FLUX MAPS

For the stator VBR formulation, some manipulation to the machine equations is required. Starting from (1), the flux derivative is written as

$$\frac{d\bar{\lambda}_{dq}}{dt} = \frac{\partial \bar{\lambda}_{dq}}{\partial \bar{i}_{dq}} \cdot \frac{d\bar{i}_{dq}}{dt} \tag{9}$$

where the partial derivative of flux with respect to current is defined as incremental inductance, thus generating the incremental inductance matrix

$$l_{dd} = \frac{\partial \lambda_d}{\partial i_d} \quad l_{dq} = \frac{\partial \lambda_d}{\partial i_q} \quad l_{qd} = \frac{\partial \lambda_q}{\partial i_d} \quad l_{qq} = \frac{\partial \lambda_q}{\partial i_q} \tag{10}$$

$$\left[l_{dq}\right] = \begin{bmatrix} l_{dd} & l_{dq} \\ l_{qd} & l_{qq} \end{bmatrix}. \tag{11}$$

It is pointed out that $[l_{dq}]$ is the matrix of the incremental inductances in the $dq$ frame, while $l_{dq}$ is one of the elements of the matrix $[l_{dq}]$ representing the cross-coupling incremental inductance between stator axis $d$ and $q$. These incremental inductances vary with the working point according to the currents. Therefore, (1) is written as follows:

$$\bar{v}_{dq} = R_s \cdot \bar{i}_{dq} + [l_{dq}] \cdot \frac{d\bar{i}_{dq}}{dt} + [J] \cdot \omega \cdot \bar{\lambda}_{dq} \tag{12}$$

where $[J] = \begin{bmatrix} 0 & -1 \\ 1 & 0 \end{bmatrix}$ is the complex operator in matrix form.

The rotational transform (13) is thus introduced as follows:

$$A(\theta) = \begin{bmatrix} \cos(\theta) & \sin(\theta) \\ -\sin(\theta) & \cos(\theta) \end{bmatrix}. \tag{13}$$

This way, by applying (13) to (12), the stationary $\alpha\beta$ voltage equations using the rotor electric position $\theta$ (see Fig. 1) are computed as follows:

$$A(-\theta)\cdot\bar{v}_{dq} = A(-\theta)\cdot R_s\cdot\bar{i}_{dq} + A(-\theta)\cdot[l_{dq}]\cdot\frac{d\bar{i}_{dq}}{dt} + A(-\theta)\cdot[J]\cdot\omega\cdot\bar{\lambda}_{dq} \Rightarrow$$

$$\bar{v}_{\alpha\beta} = R_s\cdot\bar{i}_{\alpha\beta} + A(-\theta)\cdot[l_{dq}]\cdot\frac{d\bar{i}_{dq}}{dt} + A(-\theta)\cdot[J]\cdot\omega\cdot\bar{\lambda}_{dq}. \tag{14}$$

Considering only the second term, characterized by the current derivative, (14) is transformed in

$$\begin{aligned} A(-\theta)\cdot[l_{dq}]\cdot\frac{d}{dt}\bar{i}_{dq} &= A(-\theta)\cdot[l_{dq}]\cdot\frac{d}{dt}A(\theta)\cdot\bar{i}_{\alpha\beta} \\ &= A(-\theta)\cdot[l_{dq}]\cdot A(\theta)\cdot\frac{d}{dt}\bar{i}_{\alpha\beta} \\ &\quad + A(-\theta)\cdot[l_{dq}]\cdot\frac{d}{dt}A(\theta)\cdot\bar{i}_{\alpha\beta}. \end{aligned} \tag{15}$$

The first part is equivalent to the matrix of incremental inductance in $\alpha\beta$-axes as shown as follows:

$$[l_{\alpha\beta}] = A(-\theta)\cdot[l_{dq}]\cdot A(\theta). \tag{16}$$

Since $l_{dq} = l_{qd}$ [28], each component of this matrix is calculated as follows:

$$[l_{\alpha\beta}] = \begin{bmatrix} l_{\alpha\alpha} & l_{\alpha\beta} \\ l_{\beta\alpha} & l_{\beta\beta} \end{bmatrix} = \begin{bmatrix} \cos(\theta) & -\sin(\theta) \\ \sin(\theta) & \cos(\theta) \end{bmatrix}\cdot\begin{bmatrix} l_{dd} & l_{dq} \\ l_{dq} & l_{qq} \end{bmatrix}\cdot\begin{bmatrix} \cos(\theta) & \sin(\theta) \\ -\sin(\theta) & \cos(\theta) \end{bmatrix} \tag{17}$$

$$l_{\alpha\alpha} = l_{dd}\cdot\cos^2(\theta) + l_{qq}\cdot\sin^2(\theta) - 2\cdot l_{dq}\cdot\cos(\theta)\cdot\sin(\theta) \tag{18}$$

$$l_{\alpha\beta} = l_{\beta\alpha} = l_{dq}\cdot(\cos^2(\theta) - \sin^2(\theta)) + l_{dd}\cdot\cos(\theta)\cdot\sin(\theta) - l_{qq}\cdot\cos(\theta)\cdot\sin(\theta) \tag{19}$$

$$l_{\beta\beta} = l_{qq}\cdot\cos^2(\theta) + l_{dd}\cdot\sin^2(\theta) + 2\cdot l_{dq}\cdot\cos(\theta)\cdot\sin(\theta). \tag{20}$$

It is pointed out that $[l_{\alpha\beta}]$ is the matrix of the incremental inductances in the $\alpha\beta$ frame, while $l_{\alpha\beta}$ is one of the elements of the matrix $[l_{\alpha\beta}]$ representing the cross-coupling incremental inductance between $\alpha\beta$ axes.

Coming back to (15), the second term is evaluated by calculating the derivative of the rotational transform matrix

$$\frac{d}{dt}(A(\theta)) = -\omega\cdot\begin{bmatrix} \sin(\theta) & -\cos(\theta) \\ \cos(\theta) & \sin(\theta) \end{bmatrix} \tag{21}$$

where $\omega$ is the electrical speed. Therefore, the following is obtained:

$$A(-\theta)\cdot[l_{dq}]\cdot\frac{d}{dt}(A(\theta))\cdot\bar{i}_{\alpha\beta} = A(-\theta)\cdot[l_{dq}]\cdot(-\omega)\cdot\begin{bmatrix} \sin(\theta) & -\cos(\theta) \\ \cos(\theta) & \sin(\theta) \end{bmatrix}\cdot\bar{i}_{\alpha\beta}. \tag{22}$$

Considering that $\bar{i}_{\alpha\beta} = A(-\theta)\cdot\bar{i}_{dq}$, (22) becomes

$$\begin{aligned} &A(-\theta)\cdot[l_{dq}]\cdot(-\omega)\cdot \\ &\begin{bmatrix} \sin(\theta) & -\cos(\theta) \\ \cos(\theta) & \sin(\theta) \end{bmatrix}\cdot\begin{bmatrix} \cos(\theta) & -\sin(\theta) \\ \sin(\theta) & \cos(\theta) \end{bmatrix}\cdot\bar{i}_{dq} \\ &= A(-\theta)\cdot[l_{dq}]\cdot(-\omega)\cdot[J]\cdot\bar{i}_{dq}. \end{aligned} \tag{23}$$

Therefore, the stator equation $\alpha\beta$-model is written as follows:

$$\begin{aligned} \bar{v}_{\alpha\beta} &= R_s\cdot\bar{i}_{\alpha\beta} + [l_{\alpha\beta}]\cdot\frac{d\bar{i}_{\alpha\beta}}{dt} \\ &\quad + A(-\theta)\cdot[l_{dq}]\cdot(-\omega)\cdot[J]\cdot\bar{i}_{dq} + A(-\theta)\cdot[J]\cdot\omega\cdot\bar{\lambda}_{dq} \\ &= R_s\cdot\bar{i}_{\alpha\beta} + [l_{\alpha\beta}]\cdot\frac{d\bar{i}_{\alpha\beta}}{dt} \\ &\quad + A(-\theta)\cdot\{[l_{dq}]\cdot(-\omega)\cdot[J]\cdot\bar{i}_{dq} + [J]\cdot\omega\cdot\bar{\lambda}_{dq}\}. \end{aligned} \tag{24}$$

The last term in brackets is equivalent to the back-electromotive force in $dq$-axes. By multiplying the latter with the rotational transformation matrix $A(-\theta)$, this term becomes the back-electromotive force in $\alpha\beta$-axes

$$\bar{e}_{\alpha\beta} = A(-\theta)\cdot\overbrace{\{[l_{dq}]\cdot(-\omega)\cdot[J]\cdot\bar{i}_{dq} + [J]\cdot\omega\cdot\bar{\lambda}_{dq}\}}^{\bar{e}_{dq}} \tag{25}$$

$$\bar{v}_{\alpha\beta} = R_s\cdot\bar{i}_{\alpha\beta} + [l_{\alpha\beta}]\cdot\frac{d\bar{i}_{\alpha\beta}}{dt} + \bar{e}_{\alpha\beta}. \tag{26}$$

To transform equation (26) in $abc$ coordinates, it is necessary to add the zero-sequence component as follows:

$$\bar{v}_{\alpha\beta0} = \begin{bmatrix} v_\alpha \\ v_\beta \\ v_0 \end{bmatrix}\quad \bar{i}_{\alpha\beta0} = \begin{bmatrix} i_\alpha \\ i_\beta \\ i_0 \end{bmatrix}\quad \bar{e}_{\alpha\beta0} = \begin{bmatrix} e_\alpha \\ e_\beta \\ e_0 \end{bmatrix}. \tag{27}$$

The contribution of the leakage inductance ($L_{ls}$) can be added in the zero sequence of the inductance matrix $[l_{\alpha\beta}]$. The proposed elaboration neglects $L_{ls}$ in this step to have a separate term representing the leakage flux for clarity of explanation. So, the $3\times3$ $[l_{\alpha\beta0}]$ matrix is

$$\left[l_{\alpha\beta0}\right] = \begin{bmatrix} l_{\alpha\alpha} & l_{\alpha\beta} & 0 \\ l_{\alpha\beta} & l_{\beta\beta} & 0 \\ 0 & 0 & 0 \end{bmatrix}. \tag{28}$$

Then, the inverse Clarke transform $[T]^{-1}$ is applied considering also the zero sequence component as follows:

$$[T]^{-1}\cdot\bar{v}_{\alpha\beta0} = R_s\cdot[T]^{-1}\cdot\bar{i}_{\alpha\beta0}+[T]^{-1}\cdot[l_{\alpha\beta0}]\cdot\frac{d\bar{i}_{\alpha\beta0}}{dt}+[T]^{-1}\cdot\bar{e}_{\alpha\beta0} \tag{29}$$

where the Clarke transform $[T]$ is

$$\left[T\right]=\frac{2}{3}\begin{bmatrix}1 & -1/2 & -1/2\\ 0 & \sqrt{3}/2 & -\sqrt{3}/2\\ 1/2 & 1/2 & 1/2\end{bmatrix}. \tag{30}$$

Consequently, (29) is equal to

$$v_{abc}=R_s\cdot i_{abc}+[T]^{-1}\cdot[l_{\alpha\beta0}]\cdot\frac{d\bar{i}_{\alpha\beta0}}{dt}+e_{abc}. \tag{31}$$

Taking in account that $\bar{i}_{\alpha\beta0}=[T]\cdot i_{abc}$ and the Clarke transform is time-independent, (31) can be written as follows:

$$v_{abc}=R_s\cdot i_{abc}+[T]^{-1}\cdot[l_{\alpha\beta0}]\cdot[T]\cdot\frac{di_{abc}}{dt}+e_{abc} \tag{32}$$

where

$$l_{abc}=\begin{bmatrix}l_{aa} & l_{ab} & l_{ac}\\ l_{ba} & l_{bb} & l_{bc}\\ l_{ca} & l_{cb} & l_{cc}\end{bmatrix}=[T]^{-1}\cdot[l_{\alpha\beta0}]\cdot[T]. \tag{33}$$

Finally, the terms of the matrix of incremental inductances in *abc* are as follows:

$$\begin{aligned}
l_{aa}&=\frac{2}{3}\cdot l_{\alpha\alpha}\\
l_{ab}=l_{ba}&=\frac{1}{3}\cdot\left[-l_{\alpha\alpha}+\sqrt{3}\cdot l_{\alpha\beta}\right]\\
l_{ac}=l_{ca}&=\frac{1}{3}\cdot\left[-l_{\alpha\alpha}-\sqrt{3}\cdot l_{\alpha\beta}\right]\\
l_{bb}&=\frac{1}{3}\cdot\left[\frac{l_{\alpha\alpha}}{2}+\frac{3}{2}\cdot l_{\beta\beta}-\sqrt{3}\cdot l_{\alpha\beta}\right]\\
l_{bc}=l_{cb}&=\frac{1}{3}\cdot\left[\frac{l_{\alpha\alpha}}{2}-\frac{3}{2}\cdot l_{\beta\beta}\right]\\
l_{cc}&=\frac{1}{3}\cdot\left[\frac{l_{\alpha\alpha}}{2}+\frac{3}{2}\cdot l_{\beta\beta}+\sqrt{3}\cdot l_{\alpha\beta}\right].
\end{aligned} \tag{34}$$

The contribution of leakage inductance is now added to the (32), obtaining

$$v_{abc}=R_s\cdot i_{abc}+L_{ls}\cdot\frac{di_{abc}}{dt}+[l_{abc}]\cdot\frac{di_{abc}}{dt}+e_{abc}. \tag{35}$$

The (35) represents the stator-VBR formulation exploiting the flux maps elaboration.

### B. PROPOSED FULL-VBR FORMULATION

The above-described VBR formulation can reproduce only the behavior of the stator of an EESM with an imposed rotor field current. To integrate the rotor field circuit contribution, the flux derivative formulation (9) has to be extended considering the rotor current derivative. Equation (9) is further elaborated considering a frame composed by the stator $dq0$ axes and rotor axis ($dq0$, $f$). It becomes

$$\bar{\lambda}_{dq0,f}=\begin{bmatrix}\lambda_d\\ \lambda_q\\ \lambda_0\\ \lambda_f\end{bmatrix}\quad \bar{i}_{dq0,f}=\begin{bmatrix}i_d\\ i_q\\ i_0\\ i_f\end{bmatrix} \tag{36}$$

$$\frac{d\bar{\lambda}_{dq0,f}}{dt}=\frac{\partial\bar{\lambda}_{dq0,f}}{\partial\bar{i}_{dq0,f}}\cdot\frac{d\bar{i}_{dq0,f}}{dt}. \tag{37}$$

The cross-coupling incremental inductances between the stator $dq0$ axes and the rotor field circuit and rotor self inductance (38) appear and need to be added to the inductance matrix (11)

$$\begin{aligned}
l_{df}&=\frac{\partial\lambda_d}{\partial i_f}\quad l_{qf}=\frac{\partial\lambda_q}{\partial i_f}\\
l_{fd}&=\frac{\partial\lambda_f}{\partial i_d}\quad l_{fq}=\frac{\partial\lambda_f}{\partial i_q}\quad l_{ff}=\frac{\partial\lambda_f}{\partial i_f}.
\end{aligned} \tag{38}$$

The complete incremental inductance matrix in a $dq0,f$ frame, including also the leakage inductance ($L_{ls}$) to have a more compact form, becomes

$$\begin{aligned}
\frac{d}{dt}\begin{bmatrix}\lambda_d\\ \lambda_q\\ \lambda_0\\ \lambda_f\end{bmatrix}&=\begin{bmatrix}l_{dd} & l_{dq} & 0 & l_{df}\\ l_{qd} & l_{qq} & 0 & l_{qf}\\ 0 & 0 & L_{ls} & 0\\ l_{fd} & l_{fq} & 0 & l_{ff}\end{bmatrix}\cdot\frac{d}{dt}\begin{bmatrix}i_d\\ i_q\\ i_0\\ i_f\end{bmatrix}\\
&=\left[l_{dq0,f}\right]\cdot\frac{d\bar{i}_{dq0,f}}{dt}.
\end{aligned} \tag{39}$$

The partial derivatives of (10) and (38) can be elaborated from the flux maps and stored in inductances maps. The $d-f$ incremental inductances of the EESM motor under consideration are shown in Fig. 6.

To derive the new VBR model in ($abc$, $f$) frame, it is necessary to apply to (39) an extended version of the Park transformation matrix ($[K]$) that takes into account also the rotor terms (40)

$$\left[K\right]=\frac{2}{3}\begin{bmatrix}\cos(\theta) & \cos(\theta-\frac{2}{3}\pi) & \cos(\theta+\frac{2}{3}\pi) & 0\\ -\sin(\theta) & -\sin(\theta-\frac{2}{3}\pi) & -\sin(\theta+\frac{2}{3}\pi) & 0\\ 1/2 & 1/2 & 1/2 & 0\\ 0 & 0 & 0 & 3/2\end{bmatrix}. \tag{40}$$

The rotor axis, as evidenced by (40), does not experience any transformation. Consequently, the new formulation of the

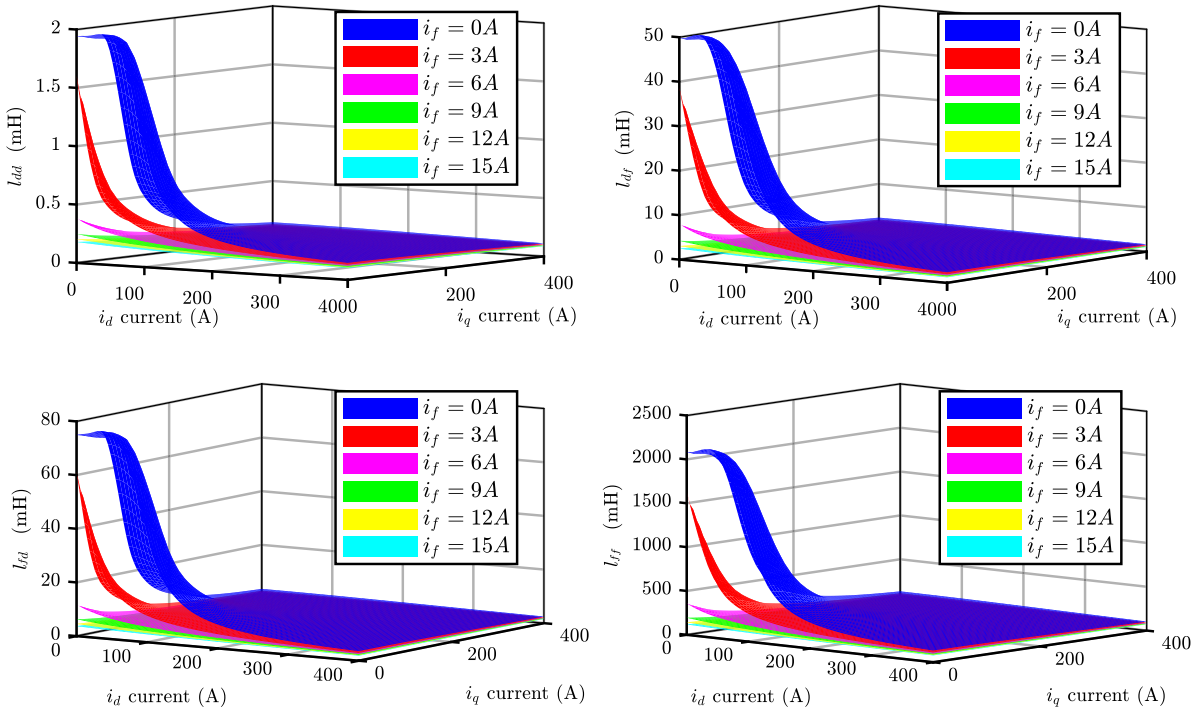


**FIGURE 6.** View of the $d-f$ incremental inductances for the EESM under test.

incremental inductance matrix in the $(abc, f)$ form becomes

$$l_{abc,f} = \begin{bmatrix} l_{aa} & l_{ab} & l_{ac} & l_{af} \\ l_{ba} & l_{bb} & l_{bc} & l_{bf} \\ l_{ca} & l_{cb} & l_{cc} & l_{cf} \\ l_{fa} & l_{fb} & l_{fc} & l_{ff} \end{bmatrix} = [K]^{-1} \cdot [l_{dq0,f}] \cdot [K]. \tag{41}$$

From (25), the $dq$ back-electromotiveforce (back-emf) is

$$\bar{e}_{dq} = [l_{dq}] \cdot (-\omega) \cdot [J] \cdot \bar{i}_{dq} + [J] \cdot \omega \cdot \bar{\lambda}_{dq}. \tag{42}$$

To complete the VBR model, the back-emf is also elaborated considering the frame $dq0$, $f$ as follows:

$$\bar{e}_{dq0,f} = [l_{dq0,f}] \cdot (-\omega) \cdot [J_{4\times4}] \cdot \bar{i}_{dq0,f} + [J_{4\times4}] \cdot \omega \cdot \bar{\lambda}_{dq0,f}. \tag{43}$$

Recalling from (23) that $[J] = \frac{dA(\theta)}{dt} \cdot A(-\theta)$ and that the rotor axis does not experience any rotation from $dq0$, $f \rightarrow abc$, $f$, the extended $[J]$ becomes

$$\begin{bmatrix} -\sin(\theta) & \cos(\theta) & 0 & 0 \\ -\cos(\theta) & -\sin(\theta) & 0 & 0 \\ 0 & 0 & 0 & 0 \\ 0 & 0 & 0 & 0 \end{bmatrix} \cdot \begin{bmatrix} \cos(\theta) & -\sin(\theta) & 0 & 0 \\ \sin(\theta) & \cos(\theta) & 0 & 0 \\ 0 & 0 & 1 & 0 \\ 0 & 0 & 0 & 1 \end{bmatrix}$$

$$= [J_{4\times4}] = \begin{bmatrix} 0 & -1 & 0 & 0 \\ 1 & 0 & 0 & 0 \\ 0 & 0 & 0 & 0 \\ 0 & 0 & 0 & 0 \end{bmatrix}. \tag{44}$$

A voltage component, behaving as an equivalent back-emf (43), appears also in the rotor equivalent circuit and is defined accordingly as follows:

$$e_f = (l_{fd} \cdot i_q - l_{fq} \cdot i_d) \cdot \omega. \tag{45}$$

This contribution appears in the VBR formalization to depict the armature reaction, i.e., the effect of the stator currents induced voltage on the rotor circuit. Applying to (43) the transformation matrix $[K]$ (40), it is obtained $e_{abc,f}$. The final voltage equation in $abc$, $f$ form is

$$v_{abc,f} = R_s \cdot i_{abc,f} + [l_{abc,f}] \cdot \frac{di_{abc,f}}{dt} + e_{abc,f}. \tag{46}$$

The proposed Full-VBR elaboration scheme for an EESM is shown in Fig. 7. Stator and rotor circuits are electrically separated but magnetically coupled.

## V. STATOR LEAKAGE INDUCTANCE COMPUTATION

In the proposed VBR model, no assumptions on the leakage inductance derivation is made as any strategy can be potentially employed [25]. However, there are some applications where a precise estimation of the stator leakage inductance is fundamental. Indeed, in the case of nonisolated neutral or dual-bridge inverter supply [40], the behavior of the zero sequence current must be simulated accurately, thus requiring an accurate estimate of the stator leakage inductance. Therefore, an additional goal of this article is to propose an accurate analytical computation of this parameter, obtained by manipulating the direct flux maps properly.

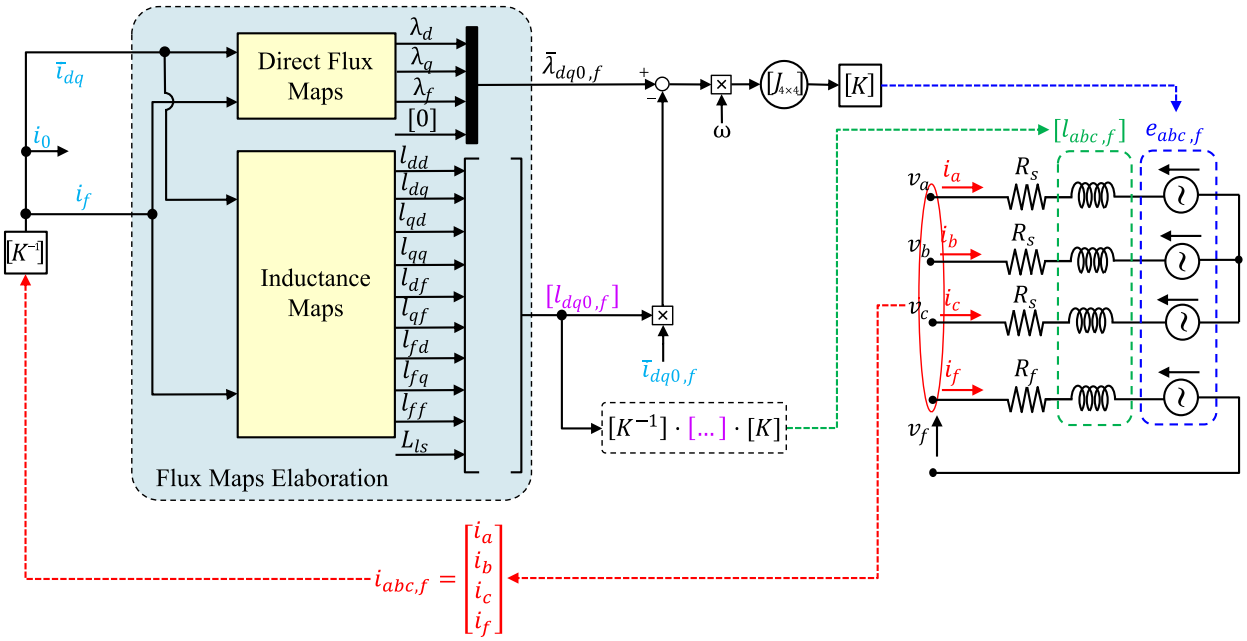


**FIGURE 7.** Proposed full-VBR model scheme for a EESM.

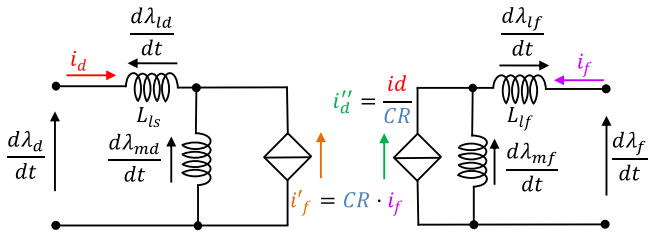


**FIGURE 8.** Equivalent circuit of the EESM considering the cross-coupling with the field circuit (stator and rotor resistances are not reported for simplicity).

The proposed procedure to identify the stator leakage inductance is based on the equivalent circuit reported in Fig. 8, where the apex $'$ is used to refer the rotor current to the stator magnetic circuit while the apex $''$ is used to refer the stator current to the rotor magnetic circuit. The computation of stator leakage inductance is performed in sequential steps reported in the following.

1) The rotor and the $d$-axis stator fluxes are evaluated at zero $d$-axis stator current

$$\begin{cases} \lambda_f \mid_{i_d=0} = \lambda_f(0, i_q, i_f) \\ \lambda_d \mid_{i_d=0} = \lambda_d(0, i_q, i_f) \end{cases}. \tag{47}$$

In this condition, the $d$-axis magnetizing flux on the stator side $\lambda_{md}$ is thus evaluated as follows:

$$\lambda_{md} \mid_{i_d=0} = \lambda_d \mid_{i_d=0} - L_{ls} \cdot \overbrace{i_d}^{0} = \lambda_d \mid_{i_d=0}. \tag{48}$$

In addition, by knowing the rotor leakage inductance $L_{lf}$, which can be easily determined through FEA analysis, it is possible to calculate the magnetizing flux on the rotor side $\lambda_{mf}$ as follows:

$$\lambda_{mf} \mid_{i_d=0} = \lambda_f \mid_{i_d=0} - \lambda_{lf} \mid_{i_d=0} = \lambda_f \mid_{i_d=0} - L_{lf} \cdot i_f. \tag{49}$$

2) The rotor and the $d$-axis stator fluxes are now evaluated at zero rotor current

$$\begin{cases} \lambda_f \mid_{i_f=0} = \lambda_f(i_d, i_q, 0) \\ \lambda_d \mid_{i_f=0} = \lambda_d(i_d, i_q, 0) \end{cases}. \tag{50}$$

Consequently, the magnetizing flux on the rotor side ($\lambda_{mf}$) is straightforwardly evaluated as

$$\lambda_{mf} \mid_{i_f=0} = \lambda_f \mid_{i_f=0} - L_{lf} \cdot \overbrace{i_f}^{0} = \lambda_f \mid_{i_f=0}. \tag{51}$$

3) Let's consider the equivalent circuit of Fig. 8 in the following two scenarios.
   1) In case of zero field current ($i_f = 0$), the magnetizing rotor flux ($\lambda_{mf} \mid_{i_f=0}$) is produced only by the stator $d$-axis current referred to the rotor side, hereafter called $i''_d$.
   2) In case of zero $d$-axis stator current ($i_d = 0$), the magnetizing rotor flux ($\lambda_{mf} \mid_{i_d=0}$) is produced only by the rotor current $i_f$.

Therefore, for a given magnetizing field flux $\lambda_{mf}$, the comparison between the above scenarios allows to numerically compute $i''^*_d$ that obtain the same effect of the rotor current $i_f$:

$$i''^*_d : \lambda_{mf}(i_f) \mid_{i_d=0} = \lambda_{mf}(i''^*_d) \mid_{i_f=0}. \tag{52}$$

Although (52) is straightforward to implement numerically, it typically requires direct flux maps that span much over the maximum stator current amplitude of the motor. In fact, applying (52) requires the calculation of $i_d''^*$ by assuming that the latter exclusively produces every possible value of $\lambda_{mf}$, including operating conditions with significant magnetic saturation. It is guessed that for high values of $\lambda_{mf}$, the corresponding $i_d$ must assume very high values that overcome the conventional limits of the direct flux maps. Indeed, the rotor magnetizing flux $\lambda_{mf}$ is normally produced by the rotor current $i_f$. Conversely, (52) aims to obtain this flux $\lambda_{mf}$ just using the armature reaction $i_d''$. However, the armature reaction impacts the rotor magnetization according to the current ratio $\mathrm{CR} = i_d/i_d''$, which is strictly related to the turns ratio between stator and rotor windings, normally very high in EESMs.

4) For each combination of $i_d''^*$ and $i_q$, it is now computed the $d$-axis stator flux under the assumption that $i_d = 0$ and $i_f = i_d''^*$. In other words, it is imposed a rotor current value $i_f$ such that the $d$-axis stator flux is equal to that produced by the only $i_d''$. In this condition, the $d$-axis stator flux thus corresponds to the magnetizing one since the $d$-axis current is zero

$$\lambda_d(0, i_q, i_f = i_d''^*) = \lambda_{md}(0, i_q, i_f = i_d''^*). \quad (53)$$

However, by definition of $i_d''^*$, the following equality is valid:

$$\lambda_{md}(0, i_q, i_f = i_d''^*) = \lambda_{md}(i_d, i_q, 0) = \lambda_{md}\,|_{i_f=0}\,. \quad (54)$$

5) From (50) and (54), the stator leakage flux is now easily evaluated as follows:

$$\lambda_{ld} = \lambda_d\,|_{i_f=0} - \lambda_{md}\,|_{i_f=0}\,. \quad (55)$$

Finally, the stator leakage inductance $L_{ls}$ is computed as follows:

$$L_{ls}(i_d, i_q) = \frac{\lambda_{ld}(i_d, i_q)}{i_d}. \quad (56)$$

Considering each combination of $i_d, i_q, i_f$, using the above mentioned procedure, the map of the stator leakage flux ($\lambda_{ld}(i_d, i_q)$) is derived and so the stator leakage inductance for the $dq$-axes [$L_{ls}(i_d, i_q)$, Fig. 9]. Obviously, the inductance $L_{ls}$ is evaluated independent from $i_f$, justified by the fact that the leakage flux is only correlated with local saturation phenomenon that happens in the stator lamination.

From the proposed procedure to compute the stator leakage inductance, it is also noted that the application of (55) allows obtaining the effective CR between stator and rotor circuit. Indeed, the $CR$ is computed as follows:

$$\mathrm{CR}(i_d, i_q, i_f) = \frac{i_d}{i_d''^*}. \quad (57)$$

For the considered EESM, the computed surface of $\mathrm{CR}(i_d, i_q, i_f)$ for different rotor current ($i_f$) levels are shown in Fig. 10. It is noted that the CR is strictly dependent on the operating point and cannot be considered constant. It is highlighted that the accurate computation of the $CR$ just represents a conceptual result that, although it has never been reported in the literature, is not functional for implementing the proposed VBR model.

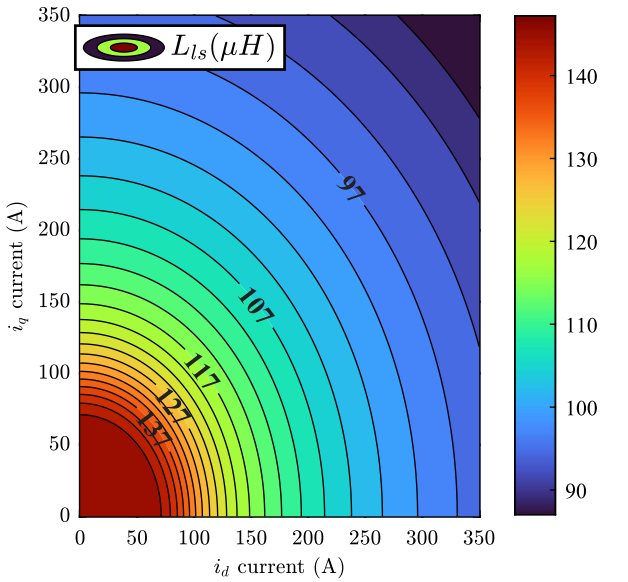


**FIGURE 9.** View of the stator leakage inductance for the EESM under test.

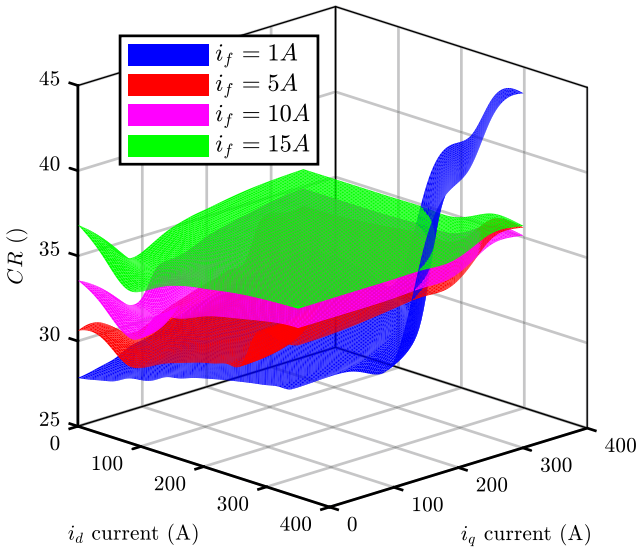


**FIGURE 10.** View of the current ratio for the EESM under test.

## VI. SIMULATION RESULTS

The proposed VBR model has been implemented in the PLECS environment, as this platform provides optimized solvers that ensure fast and accurate circuital simulations. The considered EESM is a commercial sample used on the Renault Zoe EV R135, whose main features are listed in

**TABLE 2. Primary Data of the EESM Under Test**

| | |
|---|---|
| Pole number | 4 |
| Peak power | 100 kW |
| Peak torque | 245 Nm |
| Rated dc-link voltage | 350 V |
| Peak stator current | 385 A |
| Peak rotor current | 15 A |

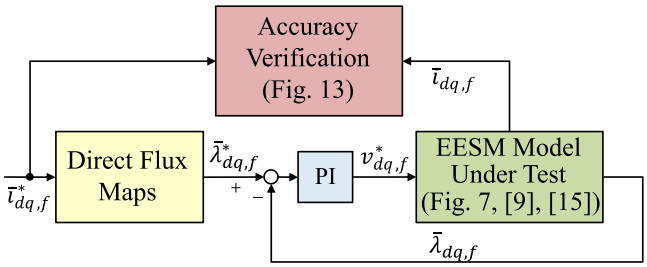


**FIGURE 11. Block diagram of the validation scheme used in the simulation environment.**

Table 2 and whose flux maps have been experimentally obtained by performing the identification procedures reported in the literature [3], [41].

The proposed VBR formulation has been compared with both inverse flux model [9] and the Full-VBR model already available in the literature [15], the latter is implemented in the PLECS environment through the block/component *"Synchronous Machine (Salient Pole, Saturable)"*. Therefore, the choice of PLECS is further justified by the possibility to perform a fair comparison between the results obtained by the proposed VBR model with those obtained by that block/component.

The flux maps have been implemented through 3-D LUTs. In detail, each direct flux map for the proposed VBR model has dimensions of $21 \times 21 \times 21$ (0.254 MB), while each inverse flux map [9] has dimensions of $101 \times 101 \times 101$ (50 MB). Indeed, to properly implement the flux-to-current relationships, the inverse flux maps require a higher number of points compared to the direct ones.

All the considered models have been simulated using PLECS's *RADAU* solver. The maximum step size has been set to 10 $\mu s$ and the relative tolerance to $1 \times 10^{-3}$. All simulations were executed on a PC running Windows 11 and equipped with a 3.8-GHz Intel CPU.

The simulation validation involves testing all possible combinations of the $dqf$ currents $(i_d^*, i_q^*, i_f^*)$ to span all the machine's operating area. These combinations are assumed as reference currents that the models must obtain as output, justifying the apex*.

The testing methodology is described in Fig. 11. First, from the reference $dqf$ currents, the corresponding reference $dqf$ fluxes $(\lambda_d^*, \lambda_q^*, \lambda_f^*)$ are computed by simply interpolating the direct flux maps. Second, from each of the tested EESM models, the effective $dqf$ fluxes $(\lambda_d, \lambda_q, \lambda_f)$ are extracted. In this way, reference- and effective- $dqf$ fluxes are compared to generate flux errors that are forced to zero using three conventional Proportional–Integral (PI) regulators (see Fig. 11). These PI regulators are ideal without any limitation in output limits and bandwidth since they must cancel the flux error without any constraint. The reasoning behind this testing approach is the following. If the $dqf$ flux errors are zero, then the $dqf$ fluxes of the EESM models correspond to their references $(\lambda_d, \lambda_q, \lambda_f) = (\lambda_d^*, \lambda_q^*, \lambda_f^*)$. However, according to the direct flux maps of the EESM, to these $dqf$ fluxes must correspond the reference $dqf$ currents $(i_d^*, i_q^*, i_f^*)$. Therefore, the correctness of each EESM model is evaluated by comparing the effective $dqf$ currents $(i_d, i_q, i_f)$ with their references. Lower is the deviation between effective- and reference- $dqf$ currents, higher is the accuracy of the considered EESM model. The block diagram of the validation scheme of each simulated EESM model is shown in Fig. 11 to help understanding. It is noted that the output of PI flux regulators correspond to the $dqf$ voltages of the motor, as normally implemented in the flux vector controllers reported in the literature [42].

Fig. 12 reports the comparison between reference- and effective $i_d, i_q, i_f$ currents of all considered EESM models: inverse flux maps [9], Full-VBR, available in PLECS [15], and the proposed VBR model. In order to span all possible combinations of $dqf$ currents, their references have been generated as follows:

$$\begin{cases} i_d^* = i_s^* \cdot \cos(\gamma^*) \\ i_q^* = i_s^* \cdot \sin(\gamma^*) \\ i_f^* = i_{f,\max} \cdot \sin(2 \cdot \pi \cdot f_{if} \cdot t) \end{cases} \tag{58}$$

where amplitude $(i_s)$ and position $(\gamma^*)$ of the stator current vector are obtained as

$$\begin{cases} i_s^* = i_{s,\max} \cdot \sin(2 \cdot \pi \cdot f_{is} \cdot t) \\ \gamma^* = \pi \cdot \sin(2 \cdot \pi \cdot f_\gamma \cdot t) \end{cases}. \tag{59}$$

The limits of stator and rotor currents have been set as $i_{s,\max} = 385$ A and $i_{f,\max} = 15$ A, in agreement with the primary EESM data in Table 2. The frequencies of the sinusoidal variations have been set as $f_{is} = 1$ Hz, $f_\gamma = 10$ Hz, $f_{if} = 0.1$ Hz.

As can be seen from the results shown in Fig. 12, the proposed Full-VBR model is able to efficiently follow the current references also under high dynamic operating conditions. Conversely, it is evident how the conventional VBR model described in [15] is not able to follow the reference currents, especially in the $d$-axis. This behavior, also visible in $abc$ coordinates, is expected since the conventional VBR model does not model the magnetic coupling between $d$-axis and rotor accurately in significant magnetic saturation conditions, as already described in Section III. However, it is noted that the conventional VBR model can correctly reproduce the EESM behavior in all the regions, where the magnetic saturation is not significant. In contrast, the inverse flux map model gets

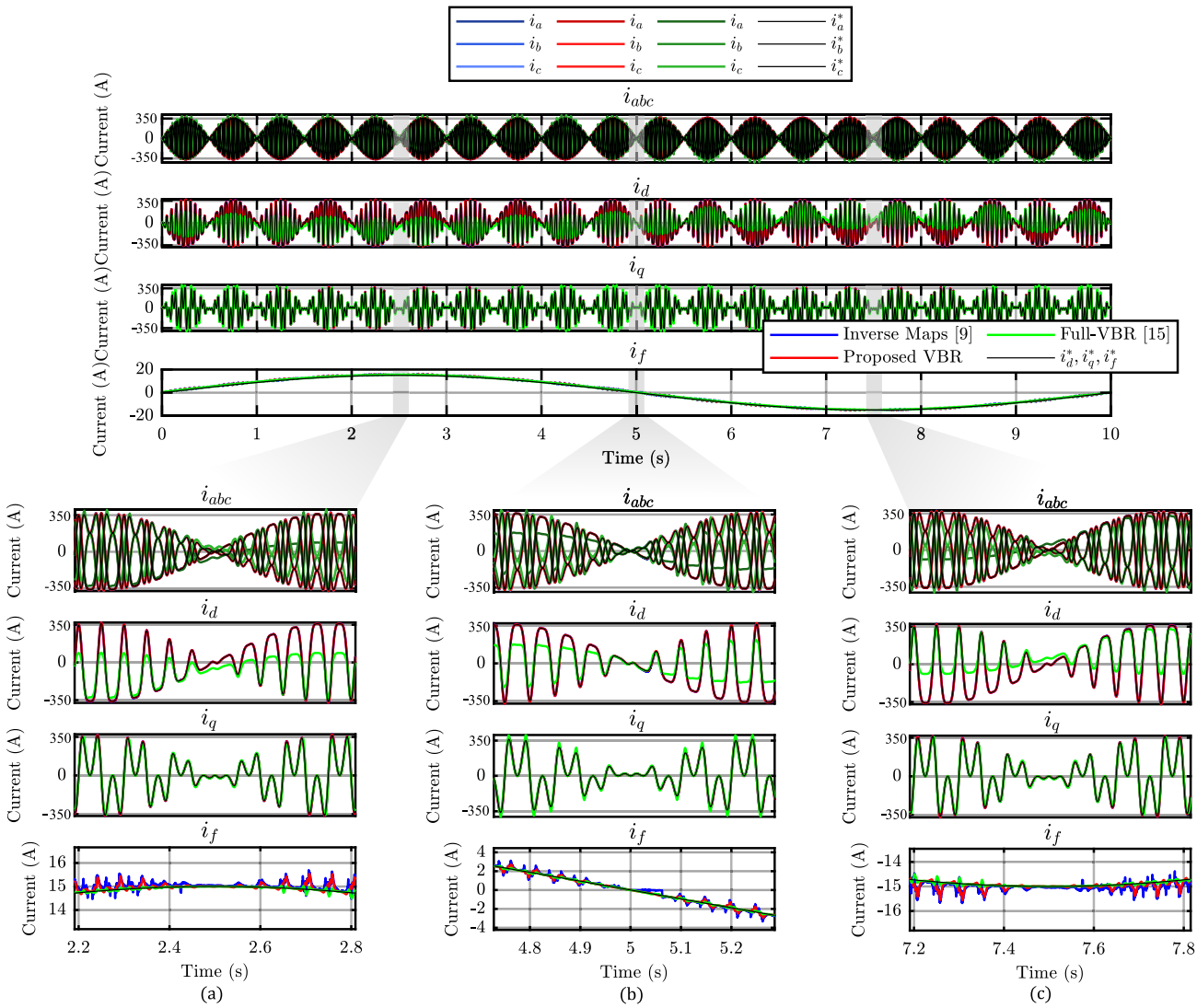


**FIGURE 12.** Accuracy verification of EESM models in simulation environment. (a) Maximum positive rotor current. (b) Zero rotor current. (c) Maximum negative rotor current.

the same results as the proposed VBR model, although it does not correspond to a circuital representation of the EESM. However, the inverse flux map model is useful to validate the proposed procedure to compute the stator leakage inductance as it automatically models the stator leakage flux by definition.

Therefore, to validate the profile of the stator leakage inductance identified in the Section V, a comparison between the inverse flux maps model and the proposed VBR one, with and without the stator leakage inductance, is performed as follows. The same test previously described and summarized in Fig. 11 is carried out. The proposed VBR model is first simulated by setting the stator leakage inductance to zero, and then simulated by implementing the profile shown in Fig. 9. The obtained result is shown in Fig. 13, where a magnification of the $d$-axis stator current is reported when it reaches the maximum value. It is noted that the implementation of the stator leakage flux using the proposed procedure allows obtaining simulation results similar and even smoother to those obtained by the inverse flux maps model. This outcome is considered a strong validation proof of the proposed procedure to compute the stator leakage inductance.

A comparison between the tested models has also been done in terms of computational time for the execution of the above-described simulation test. The faster model resulted in the inverse maps model [9], requiring an execution time of 12 s. The Full-VBR model required 1 min and 32 s. Finally, the proposed VBR model required 1 min and 53 s. These results are justified by the fact that the inverse maps model [9] does not implement any circuit. Therefore, only LUTs interpolations and algebraic computations are implemented, leading to a significantly lower execution time. It is noted that the execution time of the VBR models is comparable. In detail, the Full-VBR model [15] resulted in being slightly faster since it relies on fixed parameters in contrast

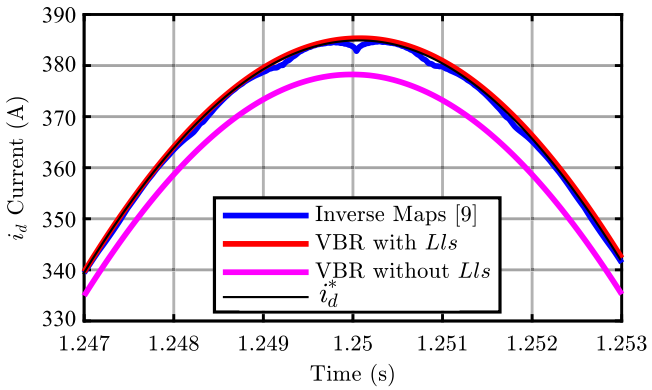


**FIGURE 13.** Accuracy verification of EESM models in simulation environment. Magnification.

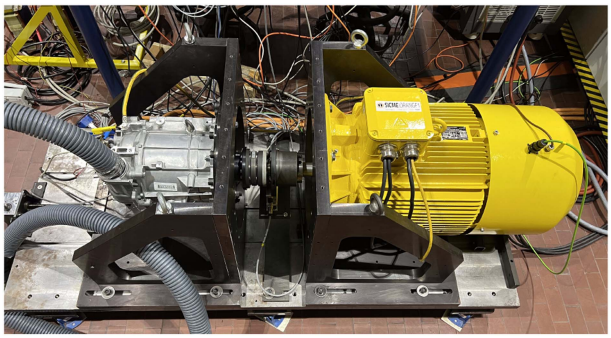

**FIGURE 14.** View of the test rig: EESM under test (left), torque transducer (center), driving machine (right).

to the proposed one, which has variable circuit parameters, justifying the higher execution time. However, the higher execution time of the proposed VBR model compared to the Full-VBR one is justified by the better accuracy, especially in significant magnetic saturation conditions.

## VII. EXPERIMENTAL VALIDATION

The experimental validation of the proposed VBR model has been performed using the same EESM adopted in the simulation section. Therefore, the machine under test (MUT) is the commercial EESM used on the Renault Zoe EV R135 (see Table 2).

### A. TEST RIG

The MUT has been mechanically coupled to a driving machine (DM) acting as a prime mover, as shown in Fig. 14. In this way, it has been possible to test the MUT directly in both current and torque control modes. Moreover, the torque sensor T40B from HBK has been mounted between MUT and DM to compare the effective MUT torque with that obtained by the proposed VBR model. The MUT has been fed by a three-phase inverter based on an insulated gate bipolar transistor (IGBT) power module. In turn, the inverter has been supplied at 350 V by a bidirectional dc source. The switching frequency of the inverter has been set at 5 kHz, with a dead time of 5 $\mu$s. In parallel, the rotor winding has been fed by an IGBT-based full-bridge dc/dc converter supplied by the same dc source before mentioned. The switching frequency of this converter has been set at 20 kHz with a dead time of 500 ns. The controllers of the stator and rotor converters consist of two dSPACEMicroLabBox units whose sampling frequencies have been set equal to the switching ones of the corresponding converters (single-edge PWM). Finally, the torque and current control algorithms used to test the EESM have been developed in MATLAB/Simulink with automatic C-code generation performed by the dSPACE controller units.

The measurement setup of the electrical quantities consists of current and voltage sensing. In detail, the MUT currents have been measured using high-bandwidth closed-loop Hall-effect transducers IT 605-S ULTRASTAB from LEM. The PWM line-to-line voltages have been instead sensed using shielded cables connected to the high-voltage and high-resolution voltage cards GN610B from HBK GmbH. Finally, all measurements have been sampled and stored using the calibrated transient recorder and data acquisition system GEN7tA from HBK GmbH, adopting a sampling frequency of 2 MS/s.

### B. EXPERIMENTAL RESULTS

Two meaningful digital twin tests have been performed to validate the proposed VBR model experimentally. The term digital twin is justified since the experimental validation provides the proposed VBR model with the same input of line-to-line voltages and mechanical speed of the MUT. In this way, it is possible to compare the corresponding outputs of mechanical torque, stator phase, and rotor currents instantaneously. The following tests have been performed:

1) Armature reaction
2) Fast torque transient

#### 1) ARMATURE REACTION TEST

The added value of the proposed VBR formulation is the capability to reproduce the cross-coupling between stator and rotor windings. The following test has been performed to validate this feature. The rotor winding has been operated in open circuit to force the corresponding current to zero. In parallel, the stator $dq$ currents have been controlled using a conventional current vector controller (CVC). Using the CVC, the $q$-axis stator current has been controlled at zero. In contrast, the $d$-axis stator current has been controlled to emphasize the armature reaction as much as possible. Therefore, the $d$-axis stator current has been first imposed to 400 A and subsequently reversed to $-400$ A according to a predefined rate of 800 A/s. The rate value is a tradeoff between the need to induce significant back-emf voltage on the rotor and having a proper time window to measure it. Therefore, for this test, the induced voltage measured on the rotor should be compared with that obtained by the proposed VBR model.

Nevertheless, this comparison is very tricky to perform. Indeed, because the $dq$ currents are controlled using a PWM

inverter, the current ripple on the stator phase currents induces PWM voltage noise on the rotor back-emf waveform. This issue is easily solved in the PLECS environment since average voltage source inverter blocks/components are available, allowing the avoidance of PWM ripple. A similar advantage is obtained using any FEA software since the profile of the $dq$ currents can be directly imposed and the induced rotor voltage can be computed by performing simple magnetostatic simulations. To solve the practical issue of removing the PWM ripple effects on the measurement of induced rotor voltage, the comparison between experimental and digital twin data has been performed as follows. According to the physical model of EESM, the $d$-axis current reversal at zero rotor current corresponds to reverse the rotor flux linkage ($\lambda_f$)

$$\lambda_f(i_d, i_q, 0) = -\lambda_f(-i_d, i_q, 0). \tag{60}$$

Therefore, according to (60) and (4), the following integral equation is valid:

$$\int_{t_a}^{t_b} v_f \, d\tau = \int_{t_a}^{t_b} \frac{d\lambda_f}{dt} \, d\tau = \lambda_f(t_b) - \lambda_f(t_a) \tag{61}$$

where $t_a$ and $t_b$ are the time instants immediately before and after the $d$-axis current reversal, respectively. By combining (60) and (61), the rotor flux linkages evaluated at those time instants are thus correlated as

$$\lambda_f(t_b) = -\lambda_f(t_a). \tag{62}$$

Therefore, by combining (61) and (62) it is obtained the following equality:

$$\int_{t_a}^{t_b} v_f \, d\tau = -2 \cdot \lambda_f(t_a) \Rightarrow \lambda_f = -\frac{\int_{t_a}^{t_b} v_f \, d\tau}{2}. \tag{63}$$

The experimental implementation of (63) is straightforward since any data recorder performing trapezoidal integration of measured samples can be used. Besides, applying (63) is very robust against the PWM voltage noise. Indeed, the integration performs a well-known powerful low-pass filter action. Therefore, the validation of the proposed test has been performed by comparing the rotor flux linkage value obtained experimentally with the corresponding waveforms obtained by the proposed VBR model and the abovementioned FEA simulation. The results are reported in Fig. 15. It is observed that despite the smooth reversal of the $d$-axis stator current, the measured rotor back-emf voltage remains highly noisy. However, it is noted that the profiles of the induced rotor voltage and corresponding rotor flux linkage are the same regardless of whether FEA or proposed VBR simulations are considered. Furthermore, the data tips reported in Fig. 15 show that the rotor flux linkage is effectively reversed from 9.698 to −9.698 Vs. By experimentally applying (63) on the rotor voltage samples, the value of 9.883 Vs is instead obtained. Thus, the corresponding percentage error is about 2%, which is very negligible considering the uncertainty related to voltage measurements, numerical integration, and the natural deviation between FEA flux maps and real ones. Finally, further validation is given by two additional waveforms reported

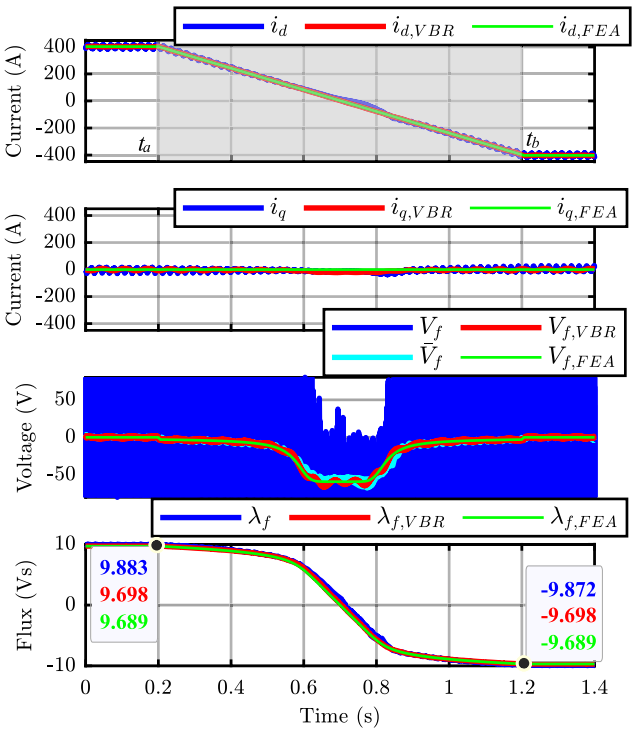


**FIGURE 15.** Armature reaction test: experimental results.

in Fig. 15. The first waveform is the moving average computation of the measured rotor voltage ($\bar{V}_f$) that nicely matches the ones obtained by the FEA simulation and VBR model. The second significant waveform is the real-time integration of the measured rotor voltage ($\lambda_f$) that shows how the experimental rotor flux linkage matches with those obtained by the proposed VBR model and FEA simulation. In summary, this digital twin test demonstrates how the proposed VBR model perfectly replicates the dynamic coupling between stator and rotor windings.

### 2) FAST TORQUE TRANSIENT

The second test to validate the proposed VBR model consisted of running it parallel to the execution of the MUT torque controller. Therefore, while executing the torque control of the machine, the line-to-line instantaneous voltages applied by the MUT converters and the mechanical speed imposed by the DM have been numerically sent in parallel to the proposed VBR model. The validation of the latter thus consisted of comparing the output currents and torque of the VBR model with those experimentally measured on the test rig. To perform a fair validation of the VBR model, a torque transient executed at low speed has been considered to make negligible the effects of skin effect, iron, and mechanical losses. The introduction of these nonidealities in the proposed VBR model indeed represents a future development of this work. The torque controller used for the MUT is based on a direct flux vector control scheme whose details are beyond this article's aim and that can be found in [21].

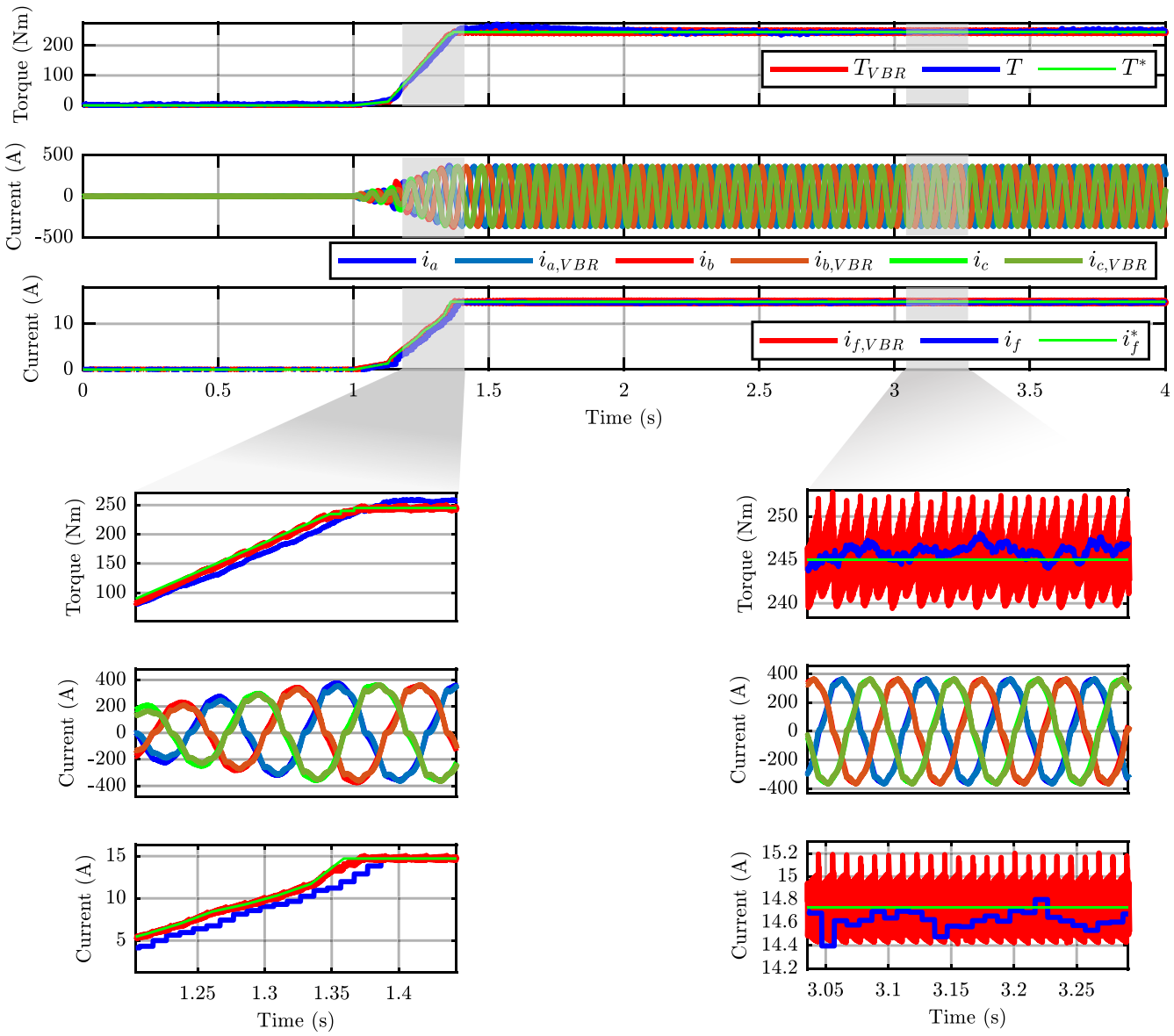


**FIGURE 16.** Fast torque transient test: experimental results.

The MUT speed has been set at 500 r/min using the DM. In order to perform a meaningful test, a fast torque transient from zero N · m up to the peak MUT torque of 245 N · m has been performed using a torque rate of 1000 Nm/s. The obtained results are shown in Fig. 16, which fully demonstrates how the proposed VBR model obtains instant-by-instant the same currents and torque measured on the test rig. Indeed, it is noted how PWM-ripple and the dead-time distortion introduced by the inverter are faithfully replicated. However, several deviations are reported in the rotor current and torque. Indeed, it is noted how the experimental rotor current is delayed with respect to that obtained by the proposed VBR model and its reference. This is due to a communication delay that affects the measurement of the rotor current. Regarding the torque, the proposed VBR model reports the PWM ripple, while the experimental measurement provides a smooth signal. This is due to the reduced bandwidth of the torque transducer, which is not able to follow the PWM ripple and the filtering of the high-frequency signal provided by the torque transducer to obtain the average value. In conclusion, this test fully demonstrates how the proposed VBR model provides accurate results in both dynamic and steady-state conditions.

## VIII. CONCLUSION

The article proposed a new VBR model for EESMs based on the current-to-flux maps to accurately depict the magnetic saturation behavior, including cross-coupling effects between stator and rotor windings. Moreover, a novel procedure for calculating the stator flux leakage and the current ratio between stator and rotor currents has been presented. Compared

to the solutions currently available in the literature, the proposed one is the first VBR EESM model able to replicate the armature reaction and the stator leakage flux accurately. The validation of the proposed VBR model has been performed both in simulation and experimental environments by considering a real commercial EESM sample for automotive application. Also, a fair simulation comparison with the EESM models reported in the literature has been performed, highlighting the added value of the proposed VBR one.

The experimental validation of the proposed VBR model was performed through digital twin tests in which the model outputs were directly compared with the experimental measurements. Experimental results confirmed the accuracy of the proposed VBR model in all operating conditions, including open rotor circuit scenario. Future development of this work will consist of the following:

1) Implementation of skin effect and iron losses phenomena to model the overall EESM efficiency accurately.
2) Implementation of the dependency of the fluxes, inductances, and torque on the rotor position to include spatial harmonics effects.

## ACKNOWLEDGMENT

The authors would like to acknowledge the financial support from the Power Electronics Innovation Center (PEIC) of Politecnico di Torino (www.peic.polito.it).

## REFERENCES

[1] A. El-Refaie and M. Osama, "High specific power electrical machines: A system perspective," *CES Trans. Elect. Machines Syst.*, vol. 3, no. 1, pp. 88–93, 2019.
[2] E. Armando, P. Guglielmi, G. Pellegrino, M. Pastorelli, and A. Vagati, "Accurate modeling and performance analysis of IPM-PMASR motors," *IEEE Trans. Ind. Appl.*, vol. 45, no. 1, pp. 123–130, Jan./Feb. 2009.
[3] E. Armando, R. I. Bojoi, P. Guglielmi, G. Pellegrino, and M. Pastorelli, "Experimental identification of the magnetic model of synchronous machines," *IEEE Trans. Ind. Appl.*, vol. 49, no. 5, pp. 2116–2125, Sep.–Oct. 2013.
[4] S. Ferrari, P. Ragazzo, G. Dilevrano, and G. Pellegrino, "Flux and loss map based evaluation of the efficiency map of synchronous machines," *IEEE Trans. Ind. Appl.*, vol. 59, no. 2, pp. 1500–1509, Mar.–Apr. 2023.
[5] X. Chen, J. Wang, B. Sen, P. Lazari, and T. Sun, "A high-fidelity and computationally efficient model for interior permanent-magnet machines considering the magnetic saturation, spatial harmonics, and iron loss effect," *IEEE Trans. Ind. Electron.*, vol. 62, no. 7, pp. 4044–4055, Jul. 2015.
[6] L. Geier, J. Stoß, A. Liske, and M. Hiller, "Generalized inversion of n-dimensional flux maps for unified nonlinear machine models and predictive control algorithms," in *Proc. IEEE Energy Convers. Congr. Expo.*, 2023, pp. 4821–4828.
[7] P. G. Carlet, L. Cinti, L. Ortombina, and N. Bianchi, "Dynamic model for HEPM motors including the nonlinear magnetic characteristics," in *Proc. IEEE Int. Electric Machines Drives Conf.*, 2023, pp. 1–7.
[8] F. Graffeo, S. Vaschetto, A. Tenconi, and A. Cavagnino, "Fast sizing procedure for salient-pole wound field synchronous motors for transportation electrification," in *Proc. IEEE Int. Electric Machines Drives Conf.*, 2023, pp. 1–7.
[9] L. Perilli, F. Graffeo, S. Rubino, and S. Vaschetto, "Dynamic models for electrically excited synchronous machines based on flux-to-current and current-to-inductance maps," in *Proc. Energy Convers. Congr. Expo.*, 2024, pp. 5588–5595.
[10] S. Pekarek, O. Wasynczuk, and H. Hegner, "An efficient and accurate model for the simulation and analysis of synchronous machine/converter systems," *IEEE Trans. Energy Convers.*, vol. 13, no. 1, pp. 42–48, Mar. 1998.
[11] Plexim, "Plecs," [Online]. Available: www.plexim.com/products/plecs
[12] L. Wang and J. Jatskevich, "A voltage-behind-reactance synchronous machine model for the emtp-type solution," *IEEE Trans. Power Syst.*, vol. 21, no. 4, pp. 1539–1549, Nov. 2006.
[13] D. Aliprantis, S. Sudhoff, and B. Kuhn, "A synchronous machine model with saturation and arbitrary rotor network representation," *IEEE Trans. Energy Convers.*, vol. 20, no. 3, pp. 584–594, Sep. 2005.
[14] D. C. Aliprantis, O. Wasynczuk, and C. D. RodrÍguez Valdez, "A voltage-behind-reactance synchronous machine model with saturation and arbitrary rotor network representation," *IEEE Trans. Energy Convers.*, vol. 23, no. 2, pp. 499–508, Jun. 2008.
[15] A. Cramer, B. Loop, and D. Aliprantis, "Synchronous machine model with voltage-behind-reactance formulation of stator and field windings," in *Proc. IEEE Power Energy Soc. Gen. Meeting*, 2013, p. 1.
[16] D. Aliprantis, S. Sudhoff, and B. Kuhn, "Experimental characterization procedure for a synchronous machine model with saturation and arbitrary rotor network representation," *IEEE Trans. Energy Convers.*, vol. 20, no. 3, pp. 595–603, Sep. 2005.
[17] S.-A. Tahan and I. Kamwa, "A two-factor saturation model for synchronous machines with multiple rotor circuits," *IEEE Trans. Energy Convers.*, vol. 10, no. 4, pp. 609–616, Dec. 1995.
[18] K. Corzine, B. Kuhn, S. Sudhoff, and H. Hegner, "An improved method for incorporating magnetic saturation in the q-d synchronous machine model," *IEEE Trans. Energy Convers.*, vol. 13, no. 3, pp. 270–275, Sep. 1998.
[19] S. Pekarek, E. Walters, and B. Kuhn, "An efficient and accurate method of representing magnetic saturation in physical-variable models of synchronous machines," *IEEE Trans. Energy Convers.*, vol. 14, no. 1, pp. 72–79, Mar. 1999.
[20] C. Rossi, D. Casadei, A. Pilati, and M. Marano, "Wound rotor salient pole synchronous machine drive for electric traction," in *Proc. 41st IAS Conf. Rec. IEEE Ind. Appl. Conf. Annu. Meeting*, vol. 3, 2006, pp. 1235–1241.
[21] A. Ionta, S. Rubino, F. Mandrile, F. Graffeo, R. Bojoi, and E. Armando, "Direct flux vector control of electrically excited synchronous machines for electrical vehicles," in *Proc. IEEE Energy Convers. Congr. Expo.*, 2024, pp. 6431–6438.
[22] A. Rambetius, S. Luthardt, and B. Piepenbreier, "Modeling of wound rotor synchronous machines considering harmonics, geometric saliencies and saturation induced saliencies," in *Proc. Int. Power Electron. Conf.*, 2014, pp. 3029–3036.
[23] S. Ferrari, G. Dilevrano, P. Ragazzo, and G. Pellegrino, "The DQ-THETA flux map model of synchronous machines," in *Proc. IEEE Energy Convers. Congr. Expo.*, 2021, pp. 3716–3723.
[24] E. S. Tahim, Z. Feng, N. Amiri, and J. Jatskevich, "High-fidelity memory-compact dynamic model of interior-permanent magnet synchronous machines for motor-drive transient simulations," in *Proc. 23rd Int. Symp.*, 2024, pp. 1–6.
[25] M. Zhang and X. Wu, "Analytical calculation and experimental measurement of DQ inductance of permanent magnet synchronous motor," in *Proc. IEEE 5th Int. Elect. Energy Conf.*, 2022, pp. 1317–1322.
[26] K. Rahman and S. Hiti, "Identification of machine parameters of a synchronous motor," *IEEE Trans. Ind. Appl.*, vol. 41, no. 2, pp. 557–565, Mar./Apr. 2005.
[27] S.-K. Sul, *Control of Electric Machine Drive Systems*. Hoboken, NJ, USA: Wiley, 2011.
[28] B. Stumberger, G. Stumberger, D. Dolinar, A. Hamler, and M. Trlep, "Evaluation of saturation and cross-magnetization effects in interior permanent-magnet synchronous motor," *IEEE Trans. Ind. Appl.*, vol. 39, no. 5, pp. 1264–1271, Sep./Oct. 2003.
[29] L. Wang et al., "Methods of interfacing rotating machine models in transient simulation programs," *IEEE Trans. Power Del.*, vol. 25, no. 2, pp. 891–903, Apr. 2010.
[30] L. Wang, J. Jatskevich, and H. W. Dommel, "Re-examination of synchronous machine modeling techniques for electromagnetic transient simulations," *IEEE Trans. Power Syst.*, vol. 22, no. 3, pp. 1221–1230, Aug. 2007.

[31] M. Chapariha, F. Therrien, J. Jatskevich, and H. W. Dommel, "Constant-parameter circuit-based models of synchronous machines," *IEEE Trans. Energy Convers.*, vol. 30, no. 2, pp. 441–452, Jun. 2015.
[32] E. Mostajeran, N. Amiri, and J. Jatskevich, "Constant-parameter voltage-behind-reactance synchronous machine models considering main flux saturation for EMTP-type programs," *IEEE Trans. Energy Convers.*, vol. 39, no. 1, pp. 400–411, Mar. 2024.
[33] S. Zarate, G. Almandoz, G. Ugalde, J. Poza, and A. J. Escalada, "Extended DQ model of a permanent magnet synchronous machine by including magnetic saturation and torque ripple effects," in *Proc. IEEE Int. Workshop Electron., Control, Meas., Signals Appl. Mechatron.*, 2017, pp. 1–6.
[34] G. Slemon, "An equivalent circuit approach to analysis of synchronous machines with saliency and saturation," *IEEE Trans. Energy Convers.*, vol. 5, no. 3, pp. 538–545, Sep. 1990.
[35] A. Gebregergis, M. H. Chowdhury, M. S. Islam, and T. Sebastian, "Modeling of permanent-magnet synchronous machine including torque ripple effects," *IEEE Trans. Ind. Appl.*, vol. 51, no. 1, pp. 232–239, Jan./Feb. 2015.
[36] T. Wisniewski, J.-C. Vannier, B. Lorcet, J. Saint-Michel, and X. Jannot, "Wound-rotor synchronous machine DQ modeling with saturation for transient analysis," in *Proc. IEEE Int. Electric Mach. Drives Conf.*, 2017, pp. 1–6.
[37] M. Chapariha, F. Therrien, J. Jatskevich, and H. W. Dommel, "Explicit formulations for constant-parameter voltage-behind-reactance interfacing of synchronous machine models," *IEEE Trans. Energy Convers.*, vol. 28, no. 4, pp. 1053–1063, Dec. 2013.
[38] F. Therrien, M. Chapariha, and J. Jatskevich, "Constant-parameter synchronous machine model including main flux saturation," *IET Electric Power Appl.*, vol. 10, no. 6, pp. 477–487, 2016. [Online]. Available: https://ietresearch.onlinelibrary.wiley.com/doi/abs/10.1049/iet-epa.2015.0447
[39] F. Therrien, L. Wang, J. Jatskevich, and O. Wasynczuk, "Efficient explicit representation of AC machines main flux saturation in state-variable-based transient simulation packages," *IEEE Trans. Energy Convers.*, vol. 28, no. 2, pp. 380–393, Jun. 2013.
[40] H. Stemmler and P. Guggenbach, "Configurations of high-power voltage source inverter drives," in *Proc. 5th Eur. Conf. Power Electron. Appl.*, vol. 5, 1993, pp. 7–14.
[41] S. Goehner et al., "Combining locked rotor and steady state tests for eesm flux linkage identification," in *Proc. IEEE 9th Southern Power Electron. Conf.*, 2024, pp. 1–6.
[42] H. A. A. Awan, S. E. Saarakkala, and M. Hinkkanen, "Flux-linkage-based current control of saturated synchronous motors," *IEEE Trans. Ind. Appl.*, vol. 55, no. 5, pp. 4762–4769, Sep./Oct. 2019.

**ALESSANDRO IONTA** (Graduate Student Member, IEEE) was born in Rome, Italy, in 1999. He received the bachelor's degree in electrical engineering and the master's degree in mechatronic engineering, in 2020 and 2022, respectively, from the Politecnico di Torino, Torino, Italy, where he is currently working toward the Ph.D. degree in electrical, electronical and communication engineering with Dipartimento Energia "G. Ferraris".

His Ph.D. topic relates on advanced control and modeling of electrical motors for traction applications, with a particular focus on electrically excited synchronous motors.

**SANDRO RUBINO** (Member, IEEE) received the M.Sc. and Ph.D. degrees in electrical engineering from Politecnico di Torino, Torino, Italy, in 2014 and 2019, respectively.

He is currently Assistant Professor with Dipartimento Energia "G. Ferraris," Politecnico di Torino. His research interests include modeling and controlling multiphase electrical machines and high-performance AC motor drives.

Dr Rubino is an Associate Editor of IEEE TRANSACTIONS ON INDUSTRY APPLICATIONS and IEEE JOURNAL OF EMERGING AND SELECTED TOPICS IN POWER ELECTRONICS. He was the recipient of four paper awards from the Industrial Drives Committee of the IEEE Industry Applications Society and two Ph.D. thesis awards from the IEEE Power & Energy Society Italy Chapter and the IEEE Industrial Electronics Society Italy Chapter, respectively.

**FEDERICA GRAFFEO** (Member, IEEE) received the B.Sc. degree in energy engineering from the Università degli Studi di Palermo, Palermo, Italy, in 2017, and the M.Sc. and Ph.D. degrees in electrical engineering from the Politecnico di Torino, Turin, Italy, in 2020, and 2023, respectively.

She is currently an Assistant Professor with the Dipartimento Energia "G. Ferraris," Politecnico di Torino. Her research interests include electromagnetic and thermal design of synchronous electrical machines for transportation applications, with a particular focus on wound field synchronous motors.

Dr. Graffeo serves as a reviewer for several IEEE Transactions and international conferences.

**RADU BOJOI** (Fellow, IEEE) received the M.Sc. degree in electrical engineering from the Technical University of Iasi, Iasi, Romania, in 1993, and the Ph.D. degree in electrical engineering from the Politecnico di Torino, Torino, Italy, in 2002.

He is currently a Full Professor of power electronics and electrical drives with the Energy Department "G. Ferraris" and Chairman of the Power Electronics Innovation Center, Politecnico di Torino.

Dr. Bojoi is the recipient of ten IEEE paper awards, being co-author of more than 200 papers covering electrical drives and power electronics for industrial applications, transportation electrification, power quality, and home appliances. He is involved in many research projects with industry aiming at obtaining new products involving emerging technologies.